

Unveiling Intrinsic Many-Body Complexity by Compressing Single-Body Triviality

Ke Liao,* Lexin Ding, and Christian Schilling†

*Faculty of Physics, Arnold Sommerfeld Centre for Theoretical Physics (ASC),
Ludwig-Maximilians-Universität München, Theresienstr. 37, 80333 München, Germany and
Munich Center for Quantum Science and Technology (MCQST), Schellingstrasse 4, 80799 München, Germany*

The simultaneous treatment of static and dynamic correlations in strongly-correlated electron systems is a critical challenge. In particular, finding a universal scheme for identifying a single-particle orbital basis that minimizes the representational complexity of the many-body wavefunction is a formidable and longstanding problem. As a contribution towards its solution, we show that the total orbital correlation actually reveals and quantifies the intrinsic complexity of the wavefunction, once it is minimized via orbital rotations. To demonstrate the power of this concept in practice, an iterative scheme is proposed to optimize the orbitals by minimizing the total orbital correlation calculated by the tailored coupled cluster singles and doubles (TCCSD) ansatz. The optimized orbitals enable the limited TCCSD ansatz to capture more non-trivial information of the many-body wavefunction, indicated by the improved wavefunction and energy. An initial application of this scheme shows great improvement of TCCSD in predicting the singlet ground state potential energy curves of the strongly correlated C_2 and Cr_2 molecule.

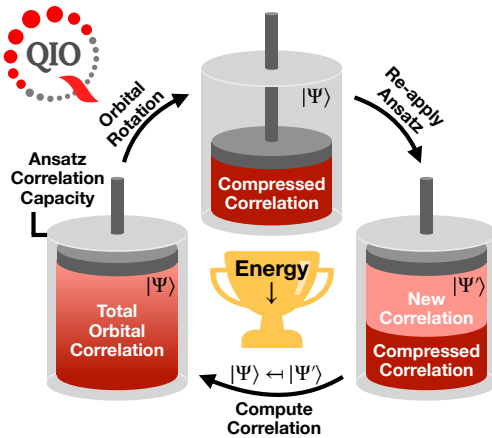


FIG. 1: TOC graphic

The *ab-initio* simulation of strongly correlated electron systems is a central challenge in quantum chemistry [1, 2] and materials science [3–5]. More specifically, this problem is complicated by the intricate interplay between the so-called static and dynamic electron-electron correlations. The former exhibits itself in the presence of many significant many-body configurations, or in the case of matrix product states (MPS) the very high bond dimensions, needed to even qualitatively describe the wavefunction. The latter includes the remaining correlation effects, such as those related to the short-range Kato cusp condition [6], long-range electron-electron screening effects [7–10], van der Waals interactions [11–13], etc. Towards solving this problem, recent years have witnessed promising developments of a plethora of methods, including tensor network theories [14–16], quantum Monte

Carlo methods [17–21], quantum chemical theories, such as specific perturbation theories [22–25], coupled cluster (CC) [26–30] and functional theories [31–34]. Each of these methods covers certain pieces of the strong correlation puzzle. Ongoing efforts are focussed on utilizing combinations of them to reach larger areas of the correlation landscape [35–41], while maintaining a delicate balance between accuracy and efficiency. In face of the complexity of the total electron correlation problem, it is surprising that the pivotal role of the underlying single-particle orbital basis is neither fully appreciated nor conclusively understood yet.

For systems dominated by dynamic correlations, the choice of the orbitals influences more the efficiency than the accuracy: Typically, orbitals from cost-effective mean-field theory like Hartree-Fock (HF) and density functional theory (DFT) are used to construct correlated many-body wavefunction ansätze; Natural orbitals, introduced by Löwdin [42], are also commonly used for a more compact Slater determinant expansion in configuration interaction (CI), CC [43–46], and explicitly correlated methods [47–51]; Localized orbitals [52, 53] are often used to achieve linear scaling with system size, exploiting the entanglement area law in gapped systems [54–56].

In systems with strong static correlations, such as systems containing transition metal elements with partially filled *d*-shells, the choice of orbitals can significantly impact not only the efficiency, but, more importantly, the accuracy. It is well recognized that the choice of the single-particle orbitals affects the representational complexity of the many-body wavefunction, e.g. in the context of the density matrix renormalization group (DMRG) [57] and full configuration interaction quantum Monte Carlo (FCIQMC) [58]. A badly chosen orbital basis can lead to an artificially difficult computational problem. For example, HF orbitals are normally too delocalized to capture strongly correlated physics, such as strong on-site Coulomb interactions and

* ke.liao.whu@gmail.com

† c.schilling@physik.uni-muenchen.de

spin fluctuations. An important advancement was the introduction of the complete active space (CAS) self-consistent field (CASSCF) method [59, 60], where both the orbitals and the CI coefficients in the active space are optimized simultaneously. Another popular choice are the natural orbitals (NO) from computationally efficient methods [37, 51, 61]. For a comprehensive review of the active space orbital construction and selection methods, we refer to Ref. [62] and the references therein [63].

As a key motivation for our work, we recall that none of the aforementioned orbitals are optimal for the total correlation problem as they are optimized for either static or dynamic correlations, but not for both. Some recognition of the importance of optimizing orbitals by taking into account both types of correlations exists at the level of single reference methods [28, 64]. Yet, a general scheme that can be easily extended to other higher-level theories is still missing. The main reason for this is the lack of a concise tool that allows one to quantify the *intrinsic complexity* of the many-body wavefunction universally, i.e., independently of the underlying ansätze. Inspired by previous work using effective quantum information concepts in quantum chemistry [65–70], it will be the accomplishment of our work to provide exactly this missing tool. To be more specific, we will establish the *total orbital correlation*, defined in (2), as a quantitative means to link the single-particle basis and the many-body wavefunction’s representational complexity, to be explained below in the next paragraphs. In particular, we will demonstrate that through minimizing the total orbital correlation one can systematically reduce the representational complexity, and hence reveal the intrinsic complexity of the many-body wavefunction. In practice, this leads to an improved accuracy of approximate ansätze like TCCSD for strongly correlated systems, as we will show in the exemplary study of the C_2 and Cr_2 molecule.

To introduce and establish the total orbital correlation as a quantitative means for describing the representational complexity of the many-body wavefunction, we first recall some basic quantum information concepts, along with an illustrative example. Given an orbital basis \mathcal{B} , and a particle number and spin conserving ground state wavefunction $|\Psi\rangle$, we can always perform the following Schmidt decomposition with respect to the bipartition between an orbital i and the rest of the orbitals, $|\Psi\rangle = \sum_{k=0,\uparrow,\downarrow,\uparrow\downarrow} \sqrt{\lambda_k^{(i)}} |k\rangle_i \otimes |\psi_k\rangle_{\setminus\{i\}}$, where $\lambda_k^{(i)}$ are the eigenvalues of the reduced density matrix ρ_i of orbital i defined as $\rho_i = \text{Tr}_{\setminus\{i\}}[|\Psi\rangle\langle\Psi|]$. Accordingly, the entropy of orbital i follows as

$$S(\rho_i) \equiv -\text{Tr}[\rho_i \log \rho_i] = - \sum_{k=0,\uparrow,\downarrow,\uparrow\downarrow} \lambda_k^{(i)} \log \lambda_k^{(i)}, \quad (1)$$

which quantifies for pure states precisely the entanglement between orbital i and the rest of the orbitals, or equivalently (up to a factor 1/2) the entire correlation including both quantum and classical contributions [71, 72].

It is worth noticing here that the eigenvalues $\lambda_k^{(i)}$ change as \mathcal{B} is varied. This can easily be seen when they are expressed as functions of the one- and two-particle reduced density matrix (1-RDM and 2-RDM) [66, 70, 73]. Moreover, the *total orbital correlation* quantifies through the quantum relative entropy $S(\rho||\sigma) \equiv \text{Tr}[\rho(\log(\rho) - \log(\sigma))]$ the deviation of the quantum state ρ (including the case of mixed states $\rho \neq |\Psi\rangle\langle\Psi|$) from the manifold of states with zero correlation between various orbitals in \mathcal{B} , i.e.

$$\begin{aligned} I_{\text{tot}}^{(\mathcal{B})}(\rho) &:= \min_{\sigma \equiv \sigma_1 \otimes \dots \otimes \sigma_d} S(\rho||\sigma) \\ &= \sum_{i=1}^M S(\rho_i) - S(\rho). \end{aligned} \quad (2)$$

In the last line, we used the well-know fact [74] that the minimum in the first line is attained for the uncorrelated state given by the product of the single orbital reduced density matrices ρ_i of ρ . In that sense $I_{\text{tot}}^{(\mathcal{B})}(\rho)$ quantifies the correlation of various M orbitals in \mathcal{B} collectively.

In order to illustrate how the total orbital correlation directly reflects the multiconfigurational character of a wavefunction $|\Psi\rangle$, we first consider a two-electron singlet state in two orbitals. In this case, the Shannon entropy of the CI coefficients of the many-body wavefunction expanded in the four configurations $\{|0, \uparrow\downarrow\rangle, |\uparrow, \downarrow\rangle, |\downarrow, \uparrow\rangle, |\uparrow\downarrow, 0\rangle\}$ is defined as $H(\{|c_i|^2\}) = -\sum_{i=1}^4 |c_i|^2 \log(|c_i|^2)$ which actually equals (up to a prefactor) the total orbital correlation (2). In particular, when the total orbital correlation is 0, the state $|\Psi\rangle$ is a single Slater determinant, whereas when it is maximal, $|\Psi\rangle$ is also maximally multiconfigurational. Remarkably, the total orbital correlation of $|\Psi\rangle$ can vary drastically when the orbital basis changes. One can ver-

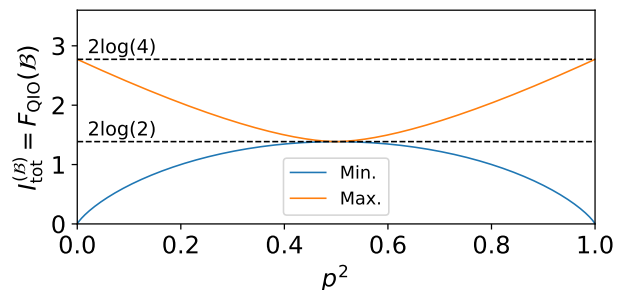


FIG. 2: Minimal and maximal total orbital correlation, Eq. (2), over all real orbital bases \mathcal{B} for a two electron singlet state $|\Psi\rangle = p|\uparrow\downarrow, 0\rangle + \sqrt{1-p^2}|0, \uparrow\downarrow\rangle$ against p^2 .

ify that it attains its minimal value for the natural orbitals of $|\Psi\rangle$ (which are in general not the minimizer), where $|\Psi\rangle$ can be expressed as a zero-seniority state $|\Psi\rangle = p|\uparrow\downarrow, 0\rangle + \sqrt{1-p^2}|0, \uparrow\downarrow\rangle$, where we use p to denote the CI coefficient of the first configuration in the natural orbital basis. We therefore define the *single-body triviality* as any redundant total orbital correlation beyond the minimal total orbital correlation, as shown as the blue

curve in Fig. 7, and the *representational complexity* as the value of the total orbital correlation in the current orbital basis. When p^2 is closed to 0 or 1, $|\Psi\rangle$ is of single reference character, and correspondingly the difference of the total orbital correlation between the “best” and “worst” choice of orbital basis is radical. When $p^2 = 1/2$, the state is equally and maximally multiconfigurational in every orbital basis, which means there is no single-body triviality in the state. For more details on this example, we refer to Appendix B.

Based on the analytic insights above, and the precise meaning of the total orbital correlation, we propose the following cost function

$$F_{\text{QIO}}(\mathcal{B}) \equiv I_{\text{tot}}^{(\mathcal{B})}(|\Psi\rangle\langle\Psi|) = \sum_{i=1}^M S(\rho_i), \quad (3)$$

where M is the total number of spatial orbitals. The minimization of (3) leads to the quantum information orbitals (QIO). The cost function is 0 when the wavefunction is a single Slater determinant, and achieves the maximal value of $M \log 4$ when the wavefunction is maximally multiconfigurational.

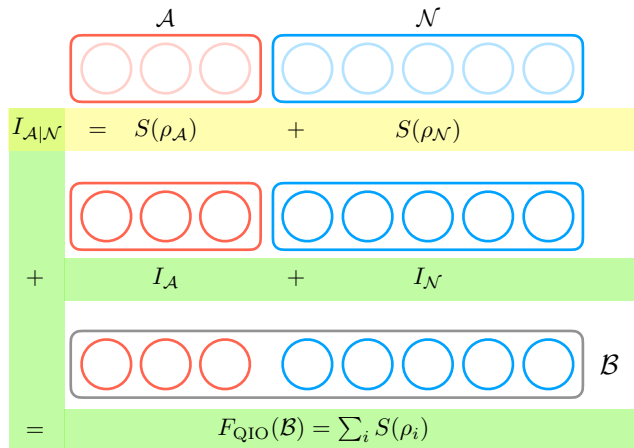


FIG. 3: Illustration of coarse-grained and finest-grained orbital correlation, and the associating sum rules (4) (terms in yellow) and (5) (terms in green).

To provide more evidence for the distinctive suitability of our cost function (3), let us first consider instead of the finest split a coarser partitioning $\Pi \equiv \mathcal{S}_1 | \dots | \mathcal{S}_R$ of the orbital basis \mathcal{B} . As an extension of Eq. (2), for any pure quantum state ρ the correlation between various subsystems \mathcal{S}_J is quantified by $I_{\Pi}(\rho) = \sum_{J=1}^R S(\rho_J)$. Here ρ_J is the orbital reduced state of subsystem \mathcal{S}_J including all orbitals $i \in \mathcal{S}_J$. This coarse-grained correlation vanishes indeed if and only if the total state ρ takes the form of a product of reduced states ρ_J of various subsystems \mathcal{S}_J . Yet, $I_{\Pi}(\rho)$ is therefore *not* capable of detecting any correlation *within* any of the subsystems \mathcal{S}_J , in striking contrast to our cost function (3) which refers to the finest partitioning of \mathcal{B} . To put this into context, we consider

the partition $\Pi = \mathcal{A}|\mathcal{N}$ of the orbitals into active and non-active spaces \mathcal{A} and \mathcal{N} , respectively, as illustrated in the first row of Figure 3. The correlation between the two subspaces is quantified as

$$I_{\mathcal{A}|\mathcal{N}} = S(\rho_{\mathcal{A}}) + S(\rho_{\mathcal{N}}). \quad (4)$$

Additionally, the two subspaces \mathcal{A} and \mathcal{N} contain internal correlations, when referring to the finest orbital partition within \mathcal{A} and \mathcal{N} (second row of Figure 3), which are quantified as $I_{\mathcal{A}/\mathcal{N}} = \sum_{i \in \mathcal{A}/\mathcal{N}} S(\rho_i) - S(\rho_{\mathcal{A}/\mathcal{N}})$. Therefore, combining the external correlation between \mathcal{A} and \mathcal{N} , and the respective internal correlation, we arrive at our cost function F_{QIO} which equals the total orbital correlation referring to the finest orbital splitting (third row in Figure 3)

$$F_{\text{QIO}}(\mathcal{B}) = \sum_i S(\rho_i) = I_{\mathcal{A}|\mathcal{N}} + I_{\mathcal{A}} + I_{\mathcal{N}}. \quad (5)$$

Accordingly, as a key insight of our work, minimizing $F_{\text{QIO}}(\mathcal{B})$ means nothing else than reducing simultaneously the correlation between the active space and the non-active space, as well as within these two subspaces.

Also from a practical point of view, our cost function is particularly suitable. To explain this, we first recall that in certain scenarios, for instance DMRG, the entropy of blocks containing more than one orbital can be efficiently exploited for orbital optimization due to the unique structure of the ansatz [57]. But, in general, going beyond the current partition will require higher order RDMs, which is computationally expensive for ansätze that do not possess the special structure of an MPS.

After having presented all these appealing features of our proposed cost function (3), one may wonder which orbitals its minimization will actually yield. Providing a comprehensive analytical answer is out of reach due to the huge complexity of the electron correlation problem and the form of (3). Yet, we recall a remarkable observation made in Ref. [75]. There, our cost function (3) was considered for spinless fermions, or equivalently for spinful fermions the total correlation with respect to the finest splitting of the one-particle Hilbert space into spin-orbitals. In that case, the minimization leads to the natural spin-orbitals, i.e., the eigenstates of the full 1-RDM including spin-information. In our case, however, the ideas of the derivation in [75] do not apply anymore. Hence, the spatial orbitals minimizing our cost function (3), termed quantum information-based orbitals (QIOs), will not coincide with the natural orbitals but they could be quite similar, at least for some systems. In that sense, our work may provide a quite surprising alternative characterization of the natural orbitals: They approximately but not exactly minimize the total orbital correlation in an N -electron wavefunction. Because of this, we will also consider the natural spatial orbitals in this work together with the QIOs obtained by minimizing (3).

Based on the above considerations, we conclude that Eq (3) is ideal for minimizing the representational com-

plexity of the many-body wavefunction from both a theoretical and practical point of view. In the remainder of the Letter, we will use the term orbital to refer to spatial orbitals only.

To turn the above theoretical insights into practical use, it is critical to calculate the 1- and 2-RDM in a both efficient and accurate way in the whole orbital space. Low-bond DMRG was used in previous studies [67, 73] for this purpose. However, in practice this approach becomes computationally expensive when the system size increases. In this Letter, we propose to use the tailored CCSD ansatz (TCCSD) [76]. This enables us to obtain the 1- and 2-RDM efficiently in the whole orbital space, as well as incorporate static and dynamic correlations simultaneously. We stress that TCCSD is used here as an example and the theoretical framework offered by this work can be applied to other ansätze as well.

TCCSD [76] was introduced to overcome the shortcomings of CCSD, namely its inadequacy in treating multireference systems, while retaining its merits at capturing dynamic correlations. Here, we focus on TCCSD paired with the complete active space CI (CASCI) solver and on the singlet ground state. First, a FCI calculation in a predefined CAS space size of $(n_e^{\text{CAS}}, n_o^{\text{CAS}})$ is performed, where n_e^{CAS} and n_o^{CAS} are the number of electrons and spatial orbitals in the CAS space, respectively. The CASCI solution $|\Psi_{\text{CAS}}\rangle$ can be expanded in the configurational basis up to a normalization prefactor as

$$|\Psi_{\text{CAS}}\rangle = c_0|D_0\rangle + \sum_{i,a \in \mathcal{A}} c_i^a \hat{a}_a^\dagger \hat{a}_i |D_0\rangle + \sum_{i,j,a,b \in \mathcal{A}} c_{ij}^{ab} \hat{a}_a^\dagger \hat{a}_b^\dagger \hat{a}_j \hat{a}_i |D_0\rangle + \dots, \quad (6)$$

where $|D_0\rangle$ is the reference determinant chosen by occupying those orbitals which have the highest occupation numbers. In the initial step, it is chosen as the Hartree-Fock determinant. In the TCCSD ansatz, the active space CI expansion coefficients c_i^a and c_{ij}^{ab} are related to the T_1^{CAS} and T_2^{CAS} amplitudes by the following expressions [76]

$$\begin{aligned} \hat{T}_1^{\text{CAS}} &= \frac{1}{c_0} \sum_{i,a \in \mathcal{A}} c_i^a \hat{a}_a^\dagger \hat{a}_i, \\ \hat{T}_2^{\text{CAS}} &= \frac{1}{c_0^2} \sum_{i,j,a,b \in \mathcal{A}} [c_0 c_{ij}^{ab} - (c_i^a c_j^b - c_j^b c_i^a)] \hat{a}_a^\dagger \hat{a}_b^\dagger \hat{a}_j \hat{a}_i. \end{aligned} \quad (7)$$

Then the TCCSD ansatz reads

$$|\Psi_{\text{TCCSD}}\rangle = \exp(\hat{T}_1^{\text{CAS}} + \hat{T}_2^{\text{CAS}} + \hat{T}_1^{\text{ext}} + \hat{T}_2^{\text{ext}}) |D_0\rangle, \quad (8)$$

where $\hat{T}_1^{\text{ext}} = \sum_{(i,a) \notin \mathcal{A}^2} T_i^a \hat{a}_a^\dagger \hat{a}_i$ and $\hat{T}_2^{\text{ext}} = \sum_{(i,j,a,b) \notin \mathcal{A}^4} T_{ij}^{ab} \hat{a}_a^\dagger \hat{a}_b^\dagger \hat{a}_j \hat{a}_i$ contain the rest of the excitations. When solving the CCSD amplitudes equations, T_1^{CAS} and T_2^{CAS} amplitudes are fixed and T_1^{ext} and T_2^{ext} amplitudes (T_i^a and T_{ij}^{ab} , respectively) are optimized.

For the purpose of our orbital optimization scheme, we need to calculate the single orbital entropy $S(\rho_i)$ from

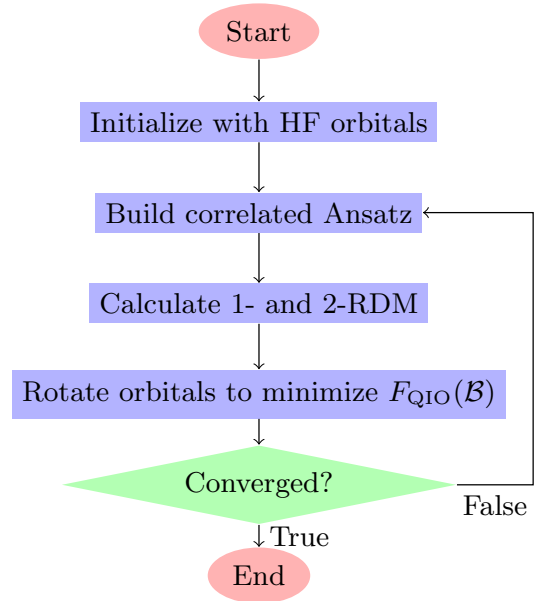


FIG. 4: Flowchart of the QIO optimization algorithm. See the main text and the Appendix A for more details.

(8). The von Neumann entropy S is only well defined for orbital reduced states ρ_i 's that are positive semi-definite, which is guaranteed if the 1- and 2-RDM, γ and Γ , respectively, are computed symmetrically via the two- and four-point correlation functions $\langle \Psi_{\text{TCCSD}} | \hat{a}_p^\dagger \hat{a}_q | \Psi_{\text{TCCSD}} \rangle$ and $\langle \Psi_{\text{TCCSD}} | \hat{a}_p^\dagger \hat{a}_q^\dagger \hat{a}_s \hat{a}_r | \Psi_{\text{TCCSD}} \rangle$ with respect to the TCCSD wavefunction (8). However, these expectations are infeasibly expensive to compute due to non-terminating commutators. To overcome this, normally the Λ -CCSD theory is used to find the left eigenstate of the similarity-transformed Hamiltonian. But the expectations now become asymmetric, because the left and right eigenstates are not the same, and the positive semi-definiteness of γ and Γ is lost in general. To allow for an efficient computation while ensuring the positive semi-definiteness, we propose to evaluate the 1- and 2-RDM as

$$\begin{aligned} \gamma_q^p &= \langle \Psi_{\text{CISD}} | \hat{a}_p^\dagger \hat{a}_q | \Psi_{\text{CISD}} \rangle, \\ \Gamma_{rs}^{pq} &= \langle \Psi_{\text{CISD}} | \hat{a}_p^\dagger \hat{a}_q^\dagger \hat{a}_s \hat{a}_r | \Psi_{\text{CISD}} \rangle, \end{aligned} \quad (9)$$

where the expectations are with respect to $|\Psi_{\text{CISD}}\rangle = \frac{1}{C} [|D_0\rangle + \sum_{i,a} T_i^a \hat{a}_a^\dagger \hat{a}_i |D_0\rangle + \sum_{i,j,a,b} (T_{ij}^{ab} + \frac{1}{2} T_i^a T_j^b) \hat{a}_a^\dagger \hat{a}_b^\dagger \hat{a}_j \hat{a}_i |D_0\rangle]$, normalized to 1 by C . The amplitudes used in $|\Psi_{\text{CISD}}\rangle$ are taken from the TCCSD ansatz, both active and non-active ones. The only caveat is that (9) neglects excitations in $|\Psi_{\text{TCCSD}}\rangle$ beyond doubles. We stress that, however, the total energy and the amplitudes are still solved for considering the full TCCSD formalism.

An iterative algorithm, consisting of macro and micro cycles as shown in Fig. 4, is employed to find the optimal orbitals by minimizing the cost function in Eq. (3). The

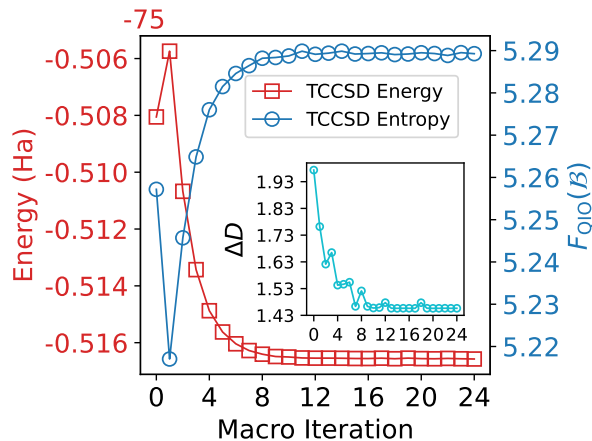


FIG. 5: TCCSD-QIO optimization of C_2 at the bond length of 6.0 Bohr (3.175 Å) in the cc-pVDZ basis set. An active space size of (8,8) is used. The inset shows the distance between the TCCSD 2-RDM and that of a nearly exact DMRG calculation, defined as $\Delta D = \sqrt{\sum_{pqrs} |\Delta\Gamma_{rs}^{pq}|^2}$. The DMRG calculation is performed using the Block2 code [77].

algorithm is initialized normally with the HF orbitals at the beginning. The minimization of the cost function is achieved by a quasi-Newton method, of which the details are presented in Appendix A. The convergence of the overall algorithm is reached when the change in the total energy is smaller than 10^{-6} Ha and the change in the cost function in the micro cycle is smaller than 10^{-7} . In practice, we use a fixed number of micro cycles (20–30) in each macro cycle, which within the initial macro cycles do not necessarily converge the cost function to the set threshold and is designed so to avoid the whole optimization getting stuck in local minima or saddle points. The overall convergence in both thresholds can be achieved by increasing the total number of macro cycles.

For comparison, we also carry out an iterative construction of the natural orbitals, substituting the step where we minimize the cost function with the step where we diagonalize the spin-traced 1-RDM to obtain NOs. In the case of TCCSD, which relies on a dominant reference determinant, an additional step of sorting the orbitals according to their occupation numbers decreasingly is needed after the orbitals are rotated and before the correlated Ansatz is built anew in the new orbital basis. The N_{act} orbitals around the Fermi level, are then chosen as the active space orbitals after the orbitals are sorted.

The Python code which achieves the QIO algorithm is available at [78]. We use PySCF [79] for obtaining the initial HF orbitals, and for creating the TCCSD algorithm. The DMRG calculations in this work are carried out by using the Block2 [77] package.

An example of the QIO algorithm in practice is shown in Fig. 5 for the orbital optimization of the C_2 at the

bond length of 6.0 Bohr (3.175 Å) in the cc-pVDZ basis set. In Appendix C we present the analogous plot for the Cr_2 molecule. Only macro iterations are shown, the micro iterations which minimize the cost function F_{QIO} are not presented. An active space size of (8,8) is used. Starting from the HF orbitals, the total orbital correlation F_{QIO} initially drops at the first macro iteration, then increases as the macro iterations proceed. Correspondingly, the total TCCSD energy first increases and then decreases. At first sight, it is counterintuitive that the total orbital correlation increases as the macro iterations proceed, since the algorithm is designed to minimize the total orbital correlation. Indeed, inside each macro iteration, the total orbital correlation is minimized through orbital rotation, while the quantum state is kept fixed. But in the next macro iteration, a new correlated TCCSD wavefunction is built based on the set of updated orbitals by solving again the amplitude equations, which allow for more correlation to be captured in the ansatz, leading to a lower energy. We interpret this increase of total orbital correlation on the level of macro iterations as a gain of non-trivial information on the many-body wavefunction level, after trivial information in the single-particle orbitals is compressed by the orbital optimization. It is worth noting that, for a FCI solution, one would not need the macro iterations. Because the FCI solution is exact in any basis and one can find the best orbital basis by minimizing the total orbital correlation, however, no more non-trivial information can be gained by doing so. Since TCCSD is not variational, a lower energy cannot be taken as better for granted. In our case, however, the lowering of the (non-variational) energy is indeed an improvement, evident by the improved wavefunction quality quantified by the distance between the TCCSD 2-RDM and that of a nearly exact DMRG calculation. The distance between the two 2-RDMs is defined as $\Delta D = \sqrt{\sum_{pqrs} |\Delta\Gamma_{rs}^{pq}|^2}$ where $\Delta\Gamma = \Gamma^{\text{TCCSD}} - \Gamma^{\text{DMRG}}$ and q, p, r, s refer to the indices of atomic orbitals. In the inset of Fig. 5, we show that the distance indeed decreases as the macro iterations proceed, thus justifying the final decreased TCCSD energy as an unmistakable improvement from the HF-TCCSD energy.

We now compare the TCCSD energy errors with various common choices of orbitals along the dissociation curve of C_2 in Fig. 6 (Left). The total orbital correlation in the optimized orbitals is also shown. All calculations are performed in the cc-pVDZ basis set, the same as in the reference DMRG calculations from Ref. [80]. Overall, the errors in the TCCSD energies using QIOs are smaller than those using HF orbitals, CASSCF-NOs and spin-averaged unrestricted CCSD natural orbitals (UCCSD-NOs). As suspected, the CASSCF-NOs, which provide the lowest active space energy, are not the optimal orbitals for the total correlation. Remarkably, in a large region along the dissociation curve, the improvement in the total energy from CASSCF-NOs/UCCSD-NOs to QIOs is as substantial as that from HF orbitals to the former. This highlights the importance of the simultaneous con-

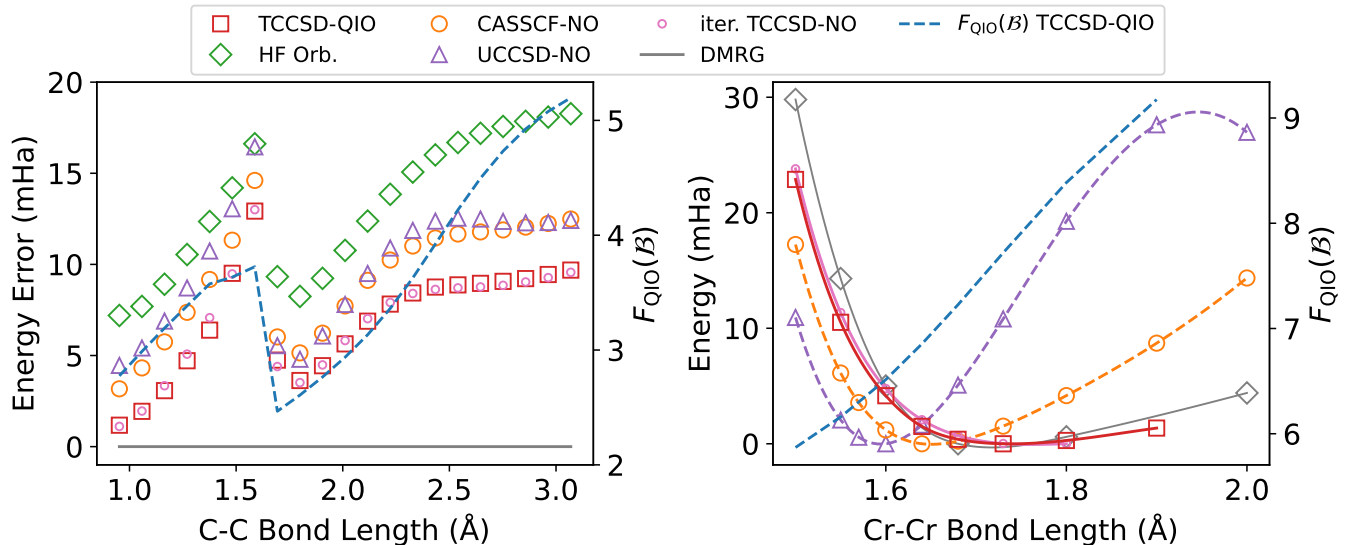


FIG. 6: (Left) TCCSD energy errors relative to nearly exact DMRG results [80] along the C_2 dissociation curve using various orbitals in the cc-pVDZ basis set. An active space size of (8,8) is used. (Right) Cr_2 potential energy curves, calculated by TCCSD and DMRG [61] in the cc-pVDZ-DK basis set. All energy curves are shifted by their respective lowest data points and are fitted using the cubic spline method. Entropies in the QIOs are shown in a blue dashed line.

sideration of static and dynamic correlations in orbital optimization. As expected, the iterative TCCSD-NOs results follow the QIO's closely, with small deviations around the equilibrium bond length. We observe that the total orbital correlation increases as the bond length increases, until it suddenly drops at the level crossing point, then increases again. We point out that the total orbital correlation is a useful indicator of the complexity of the wavefunction. For instance, it signals the level crossing point, but its value cannot be used to predict the accuracy of the TCCSD energy directly, as shown in Fig. 6 (Left). At very stretched bond lengths, the total orbital correlation is indeed larger than those at shorter bond lengths, in agreement with the intuition that the wavefunction has more multireference character at dissociation.

In Fig. 6 (Right), we show the potential energy curves of Cr_2 around the equilibrium point, calculated by TCCSD using different orbitals along with the exact DMRG results [61] in the cc-pVDZ-DK basis set. The relativistic effects are treated by using the scalar relativistic exact two-component (X2C) Hamiltonian [81, 82] as implemented in PySCF [79]. A minimal active space of (12,12) is used in TCCSD calculations. All curves are shifted by their respective lowest data points. This system has attracted extensive studies over the years [61, 83–90], and serves as a benchmark for the performance of various methods at handling strong correlations. Even around the equilibrium bond length, the ground state exhibits strong multireference characters, and to capture the shallow potential well requires also the inclusion of dynamic correlations. We note in passing that a previ-

ous study employing TCCSD has shown rather unsatisfactory results [90], i.e. a too steep potential energy well, which makes it a perfect test for QIOs.

First, we use UCCSD-NOs as done in DMRG [61]. With these orbitals, TCCSD energies yield a significantly shorter equilibrium bond length of 1.595 Å, compared to the exact DMRG result of 1.722 Å, with increasingly larger errors as the bond length increases, resulting in a very steep potential well. The TCCSD energies using CASSCF-NOs are better than using UCCSD-NOs, with a predicted equilibrium bond length of 1.651 Å. However, it yields a qualitatively wrong shape of the dissociation curve at shorter and longer bond lengths, resulting still in a too steep potential well. TCCSD in the QIOs, on the other hand, captures correctly the shallow potential well around the equilibrium point and in general improves the curve both at shorter and longer bond lengths. Especially, the equilibrium bond length predicted by TCCSD using QIO is 1.737 Å, which agrees well with the DMRG result. Most interestingly, we see a difference between the TCCSD-NOs and TCCSD-QIOs results at slightly stretched bond lengths: the former does not produce a bounded potential energy curve up until 1.8 Å, after which the iterative TCCSD-NO algorithm becomes unstable and diverges. The difference in the TCCSD energies between two stretched bond lengths is very small, therefore this unbounded behavior is more evident when we examine the energies values directly, listed in Appendix D.

As noted in Ref. [61], the ground state around 2.25 Å is particularly difficult to capture even with very high bond dimensions in DMRG. We also observe that starting from

2.0 Å, the TCCSD iterations in the QIO optimizations do not converge to the threshold of 10^{-6} in energy and the TCCSD energies oscillate between macro iterations. Therefore, we do not show the TCCSD-QIO results at bond lengths larger or equal than 2.0 Å. This likely reflects the limitations of the TCCSD ansatz with a minimal active space to represent states with very strong multireference character rather than potential shortcomings of the QIO algorithm itself. The entropy of the QIOs is shown as a blue dashed line in Fig. 6 (Right). Its smooth increase with the bond length hints at the increasing multireference character of the wavefunction, and serves as an indicator if unphysical results are obtained in the TCCSD calculations when going to larger bond lengths. As pointed out in previous studies on Cr_2 [61, 86, 88], to capture qualitatively correct the whole potential energy curve, a larger active space is needed.

We introduced a quantum information-based orbital (QIO) optimization scheme, emerging from a fresh perspective on one of the crucial steps — orbital optimization — in solving the strongly correlated many-body problem. The QIOs are characterized as those orbitals that minimize the total orbital correlation. Accordingly, they reveal the intrinsic complexity of the many-body wavefunction by compressing all trivial information into single-particle orbitals. Due to its distinctive nature, our scheme addresses the challenging task of concurrently treating both static and dynamic correlations in strongly correlated systems by optimizing orbitals considering both types of correlations. By employing our orbital optimization scheme within the TCCSD framework, we obtained superior results compared to other commonly used orbitals. The iterative orbital optimization also provides, to some extent, self-consistent feedback between the active and external space treated separately by CASCI and CCSD. This addresses partially the long-standing issue of the lack of self-consistency in the TCCSD framework. Through the lens of total orbital correlation, we also explained and demonstrated the close relationship between the QIOs and iteratively constructed NOs. The QIOs use information from both the 1- and 2-RDM, where the latter can be decomposed as $\Gamma_{rs}^{pq} = \lambda_{rs}^{pq} + \gamma_q^p \gamma_s^r - \gamma_s^p \gamma_q^r$ and λ_{rs}^{pq} is the two-body cumulant [91, 92]. The λ_{rs}^{pq} quantifies the non-trivial two-body correlation in a system. So we suspect that in more challenging cases where the two-body cumulant is non-negligible, these two types of orbitals will differ more significantly, hinted by the Cr_2 case. The computational cost of the QIO algorithm depends on the ansatz used. In the case of TCCSD, the computational cost can be broken down into three parts: i) the CASCI calculation in the active space, formally scales exponentially with the active space size; ii) the TCCSD calculation, which scales polynomially N^6 , where N is the number of electrons; and iii) the orbital optimization, which is dominated by the rotation of the 2-RDM and scales M^5 , where M is the number of orbitals. The current bottleneck in TCCSD is the limited active space size that

can be treated by CASCI, which can straightforwardly be overcome by using DMRG [93] or FCIQMC [37] as the active space solver. In the future, we hope to extend this algorithm to other systematically improvable methods, such as auxiliary-field quantum Monte Carlo (AFQMC) [20, 21, 88], as well as to spin states beyond singlets. Given the demonstrated advantages of QIOs and the comparable computational cost of QIO to CASSCF, we believe that the QIO algorithm may lead to a change of paradigm in how we approach strongly correlated many-electron systems.

Acknowledgement. We thank Huanchen Zhai and Seunghoon Lee for useful discussions on DMRG and TCCSD. We are also grateful to Ali Alavi, Daniel Kats, Stefan Knecht and Giovanni Li Manni for comments. We acknowledge financial support from the German Research Foundation (Grant SCHI 1476/1-1), the Munich Center for Quantum Science and Technology, and the Munich Quantum Valley, which is supported by the Bavarian state government with funds from the Hightech Agenda Bayern Plus.

Appendix A: Analytic Gradients, Hessians and Quasi-Newton Algorithm

The objective here is to minimize the sum of orbital entropies of all orbitals, amounting to the following cost function

$$F_{\text{QI}}(\mathcal{B}) = \sum_{i=1}^D S(\rho_i) \quad (\text{A1})$$

Let \mathbf{B} be the matrix of molecular orbital coefficients where each column corresponds to a molecular orbital. Then the transformation from the initial orbital basis \mathbf{B}_0 to the minimizing orbital basis \mathbf{B}_{opt} can be achieved by a unitary transformation $\mathbf{U}_{\text{opt}} = \exp(\mathbf{X}_{\text{opt}})$ as

$$\mathbf{B}_{\text{opt}} = \mathbf{B}_0 \mathbf{U}_{\text{opt}}^\dagger. \quad (\text{A2})$$

With the initial orbital basis fixed, e.g. the HF basis, we can denote all orbital bases by the corresponding real-value unitary \mathbf{U} or its generator, namely a skew-symmetric matrix \mathbf{X} . The set of skew-symmetric matrices can be parameterized as

$$\mathbf{X} = \sum_{i < j} x_{ij} \mathbf{A}^{(ij)} \quad (\text{A3})$$

where $\mathbf{A}^{(ij)}$ is an antisymmetric matrix with elements $A_{ij}^{(ij)} = -A_{ji}^{(ij)} = 1$ and otherwise 0. The cost function can be reparameterized as

$$F_{\text{QI}}(\mathcal{B}) \equiv F_{\text{QI}}(\mathbf{B}) = F_{\text{QI}}(\mathbf{B}_0 (e^{\mathbf{X}})^\dagger) \equiv F_{\text{QI}}(\mathbf{X}). \quad (\text{A4})$$

At a local extremum, $F_{\text{QI}}(\mathbf{X}_{\text{opt}})$ satisfies the following

extremal conditions

$$\begin{aligned} & \frac{\partial F_{\text{QI}}}{\partial x_{ij}}(\mathbf{X}_{\text{opt}}) \\ &= \lim_{\theta \rightarrow 0} \frac{F_{\text{QI}}(\mathbf{X}_{\text{opt}} + \theta \mathbf{A}^{(ij)}) - F_{\text{QI}}(\mathbf{X}_{\text{opt}})}{\theta} = 0, \end{aligned} \quad (\text{A5})$$

for all tuples (i, j) such that $i < j$. In practice, the translation invariance of the underlying $D(D-1)/2$ dimensional real space can be exploited to simplify the exponential. To be more specific, one can set the current matrix \mathbf{X} to be the origin at every gradient step, which is the same as constantly updating the reference orbital basis \mathbf{B}_0 . In that case, the derivative of the cost function simplifies to

$$\frac{\partial F_{\text{QI}}}{\partial x_{ij}}(\mathbf{0}) = \lim_{\theta \rightarrow 0} \frac{F_{\text{QI}}(\theta \mathbf{A}^{(ij)}) - F_{\text{QI}}(\mathbf{0})}{\theta}. \quad (\text{A6})$$

The infinitesimal unitary transformation $\mathbf{J}^{(ij)}(\theta) = e^{\theta \mathbf{A}^{(ij)}}$ associating to this derivative is simply a Jacobi rotation between orbital i and j :

$$\begin{aligned} (\mathbf{J}^{(ij)}(\theta))_{ii} &= \cos(\theta), \\ (\mathbf{J}^{(ij)}(\theta))_{ij} &= \sin(\theta), \\ (\mathbf{J}^{(ij)}(\theta))_{ji} &= -\sin(\theta), \\ (\mathbf{J}^{(ij)}(\theta))_{jj} &= \cos(\theta), \end{aligned} \quad (\text{A7})$$

and $(\mathbf{J}^{(ij)}(\theta))_{kl} = \delta_{kl}$ for $k, l \neq i, j$. The derivatives of F_{QI} can be further broken down using the chain rule

$$\frac{\partial F_{\text{QI}}}{\partial x_{ij}}(\mathbf{0}) = - \sum_{i=1}^D \sum_{k=0}^3 \log(\lambda_k^{(i)}(\mathbf{0})) \frac{\partial \lambda_k^{(i)}(\mathbf{0})}{\partial x_{ij}}, \quad (\text{A8})$$

where

$$\begin{aligned} \lambda_0^{(i)}(\mathbf{X}) &= 1 - \gamma(\mathbf{X})_i^i - \gamma(\mathbf{X})_{\bar{i}\bar{i}}^{\bar{i}\bar{i}} + \Gamma(\mathbf{X})_{\bar{i}\bar{i}}^{\bar{i}\bar{i}}, \\ \lambda_1^{(i)}(\mathbf{X}) &= \gamma(\mathbf{X})_i^i - \Gamma(\mathbf{X})_{\bar{i}\bar{i}}^{\bar{i}\bar{i}}, \\ \lambda_2^{(i)}(\mathbf{X}) &= \gamma(\mathbf{X})_{\bar{i}\bar{i}}^{\bar{i}\bar{i}} - \Gamma(\mathbf{X})_{\bar{i}\bar{i}}^{\bar{i}\bar{i}}, \\ \lambda_3^{(i)}(\mathbf{X}) &= \Gamma(\mathbf{X})_{\bar{i}\bar{i}}^{\bar{i}\bar{i}}. \end{aligned} \quad (\text{A9})$$

Here, $\gamma(\mathbf{X})$ and $\Gamma(\mathbf{X})$ are the 1- and 2-RDMs in the rotated basis given by

$$\begin{aligned} \gamma(\mathbf{X})_i^i &= \sum_{ab} (e^{\mathbf{X}})_{ia} (e^{\mathbf{X}})_{ib} \gamma(\mathbf{0})_b^a, \\ \Gamma(\mathbf{X})_{\bar{i}\bar{i}}^{\bar{i}\bar{i}} &= \sum_{abcd} (e^{\mathbf{X}})_{ia} (e^{\mathbf{X}})_{ib} (e^{\mathbf{X}})_{ic} (e^{\mathbf{X}})_{id} \Gamma(\mathbf{0})_{cd}^{ab}, \end{aligned} \quad (\text{A10})$$

Eventually, their derivatives at $\mathbf{0}$ can be computed from the partial derivatives of the unitary

$$\left. \frac{\partial \exp(\mathbf{X})}{\partial x_{ij}} \right|_{\mathbf{X}=\mathbf{0}} = \lim_{\theta \rightarrow 0} \frac{\mathbf{J}^{(ij)}(\theta) - \mathbb{1}}{\theta} = (\mathbf{J}^{(ij)})'(\mathbf{0}) \quad (\text{A11})$$

where

$$\begin{aligned} (\mathbf{J}^{(ij)})'(\mathbf{0})_{ii} &= 0, \\ (\mathbf{J}^{(ij)})'(\mathbf{0})_{ij} &= 1, \\ (\mathbf{J}^{(ij)})'(\mathbf{0})_{ji} &= -1, \\ (\mathbf{J}^{(ij)})'(\mathbf{0})_{jj} &= 0, \end{aligned} \quad (\text{A12})$$

with $(\mathbf{J}^{(ij)}(\theta))_{kl} = 0$ for $k, l \neq i, j$. With this we can write the derivatives of the relevant entries of the RDMs as

$$\begin{aligned} \frac{\partial \gamma(\mathbf{0})_i^i}{\partial x_{ij}} &= \gamma(\mathbf{0})_i^j + \gamma(\mathbf{0})_j^i, \\ \frac{\partial \gamma(\mathbf{0})_j^j}{\partial x_{ij}} &= -\gamma(\mathbf{0})_i^j - \gamma(\mathbf{0})_j^i, \\ \frac{\partial \Gamma(\mathbf{0})_{\bar{i}\bar{i}}^{\bar{i}\bar{i}}}{\partial x_{ij}} &= \Gamma(\mathbf{0})_{\bar{i}\bar{i}}^{j\bar{j}} + \Gamma(\mathbf{0})_{\bar{i}\bar{i}}^{i\bar{j}} + \Gamma(\mathbf{0})_{j\bar{j}}^{\bar{i}\bar{i}} + \Gamma(\mathbf{0})_{i\bar{i}}^{\bar{j}\bar{j}}, \\ \frac{\partial \Gamma(\mathbf{0})_{j\bar{j}}^{\bar{j}\bar{j}}}{\partial x_{ij}} &= -\Gamma(\mathbf{0})_{j\bar{j}}^{i\bar{i}} - \Gamma(\mathbf{0})_{j\bar{j}}^{j\bar{i}} - \Gamma(\mathbf{0})_{i\bar{i}}^{j\bar{j}} - \Gamma(\mathbf{0})_{i\bar{i}}^{j\bar{j}}. \end{aligned} \quad (\text{A13})$$

For the quasi-Newton algorithm we also need the second derivative of the cost function, which we shall approximate with its diagonal elements

$$\begin{aligned} \frac{\partial^2 F_{\text{QI}}(\mathbf{0})}{\partial x_{ij}^2} &= - \sum_{i=1}^D \sum_{k=0}^3 \left[\frac{1}{\lambda_k^{(i)}(\mathbf{0})} \left(\frac{\partial \lambda_k^{(i)}(\mathbf{0})}{\partial x_{ij}} \right)^2 \right. \\ &\quad \left. + \log(\lambda_k^{(i)}(\mathbf{0})) \frac{\partial^2 \lambda_k^{(i)}(\mathbf{0})}{\partial x_{ij}^2} \right], \end{aligned} \quad (\text{A14})$$

which involves the second derivatives of the RDMs. Again, from the second derivative of the orbital rotation matrix

$$\begin{aligned} (\mathbf{J}^{(ij)})''(\mathbf{0})_{ii} &= -1, \\ (\mathbf{J}^{(ij)})''(\mathbf{0})_{ij} &= 0, \\ (\mathbf{J}^{(ij)})''(\mathbf{0})_{ji} &= 0, \\ (\mathbf{J}^{(ij)})''(\mathbf{0})_{jj} &= -1, \end{aligned} \quad (\text{A15})$$

with $(\mathbf{J}^{(ij)}(\theta))_{kl} = 0$ for $k, l \neq i, j$, we can derive the second derivatives of the relevant entries of the RDMs

$$\begin{aligned} \frac{\partial^2 \gamma(\mathbf{0})_i^i}{\partial x_{ij}^2} &= -2\gamma(\mathbf{0})_i^i + 2\gamma(\mathbf{0})_j^j, \\ \frac{\partial^2 \gamma(\mathbf{0})_j^j}{\partial x_{ij}^2} &= 2\gamma(\mathbf{0})_i^i - 2\gamma(\mathbf{0})_j^j, \\ \frac{\partial^2 \Gamma(\mathbf{0})_{\bar{i}\bar{i}}^{\bar{i}\bar{i}}}{\partial x_{ij}^2} &= -4\Gamma(\mathbf{0})_{\bar{i}\bar{i}}^{\bar{i}\bar{i}} + 2 \sum_{(a,b,c,d) \in \mathcal{P}(i,i,j,j)} \Gamma(\mathbf{0})_{ac}^{bd}, \\ \frac{\partial^2 \Gamma(\mathbf{0})_{j\bar{j}}^{\bar{j}\bar{j}}}{\partial x_{ij}^2} &= -4\Gamma(\mathbf{0})_{j\bar{j}}^{\bar{j}\bar{j}} + 2 \sum_{(a,b,c,d) \in \mathcal{P}(i,i,j,j)} \Gamma(\mathbf{0})_{a\bar{c}}^{b\bar{d}}, \end{aligned} \quad (\text{A16})$$

where $\mathcal{P}(i, i, j, j)$ collects all permutations of the tuple (i, i, j, j) .

At each micro-iteration, the \mathbf{X} matrix is updated by the following equation

$$\mathbf{X} \leftarrow \mathbf{X} - \alpha[\mathbf{H} - (\min(\mathbf{H}) + \delta)]^{-1} \mathbf{G}, \quad (\text{A17})$$

where α (typically $0.1 - 0.3$) is the step size, \mathbf{H} is the diagonal Hessian matrix of the cost function (A14), δ is a small positive level-shift parameter ($10^{-4} - 10^{-1}$) and \mathbf{G} is the gradient of the cost function (A8).

Appendix B: Two-Electron Singlet State in Two Orbitals

Let $|\Psi\rangle$ be a two-electron singlet state in two orbitals (which form a basis \mathcal{B} of the orbital one-particle Hilbert space) associated with annihilation (creation) operators $f_{1/2\sigma}^{(\dagger)}$. Then the following form is general

$$|\Psi(\mathbf{p})\rangle = p_0|\Psi_0\rangle + p_1|\Psi_1\rangle + p_2|\Psi_2\rangle, \quad (\text{B1})$$

where

$$\begin{aligned} |\Psi_0\rangle &= f_{1\uparrow}^\dagger f_{1\downarrow}^\dagger |0\rangle, \\ |\Psi_1\rangle &= \frac{1}{\sqrt{2}}(f_{1\uparrow}^\dagger f_{2\downarrow}^\dagger - f_{1\downarrow}^\dagger f_{2\uparrow}^\dagger) |0\rangle, \\ |\Psi_2\rangle &= f_{2\uparrow}^\dagger f_{2\downarrow}^\dagger |0\rangle. \end{aligned} \quad (\text{B2})$$

Although the form of $|\Psi(\mathbf{p})\rangle$ is the most general, it is not the most concise in terms of its CI expansion, whose complexity can be measured by the Shannon entropy of the absolute squares of the CI coefficients

$$\begin{aligned} H\left(\left\{p_0^2, \frac{p_1^2}{2}, \frac{p_1^2}{2}, p_2^2\right\}\right) \\ = -p_0^2 \log(p_0^2) - p_1^2 \log\left(\frac{p_1^2}{2}\right) - p_2^2 \log(p_2^2). \end{aligned} \quad (\text{B3})$$

In this very special case, the CI entropy precisely coincide with the entanglement between the two spatial orbitals, given by the von Neumann entropy

$$S(\rho) = -\text{Tr}[\rho \log(\rho)] \quad (\text{B4})$$

of one of the orbital reduced density matrix

$$\rho_{1/2}(\mathbf{p}) = \text{Tr}_{2/1}[|\Psi(\mathbf{p})\rangle\langle\Psi(\mathbf{p})|] = \begin{pmatrix} p_0^2 & 0 & 0 & 0 \\ 0 & p_1^2/2 & 0 & 0 \\ 0 & 0 & p_1^2/2 & 0 \\ 0 & 0 & 0 & p_2^2 \end{pmatrix}. \quad (\text{B5})$$

Clearly, $S(\rho_{1/2}(\mathbf{p}))$ depends on the vector \mathbf{p} , which for a fixed state $|\Psi\rangle$ again depends on the orbital basis \mathcal{B} . We now determine the orbital basis in which the single orbital entropy as well as the multireference character of the state is minimized/maximized.

We consider all possible real orbital basis, which can be realized by a 2-by-2 orthogonal transformation from the current basis

$$\begin{aligned} f_{1\uparrow/\downarrow}^{(\dagger)} &\mapsto \cos(\theta) f_{1\uparrow/\downarrow}^{(\dagger)} - \sin(\theta) f_{2\uparrow/\downarrow}^{(\dagger)}, \\ f_{2\uparrow/\downarrow}^{(\dagger)} &\mapsto \sin(\theta) f_{1\uparrow/\downarrow}^{(\dagger)} + \cos(\theta) f_{2\uparrow/\downarrow}^{(\dagger)}. \end{aligned} \quad (\text{B6})$$

In the new orbital basis the state $|\Psi\rangle$ becomes

$$|\Psi(\mathbf{p}, \theta)\rangle = q_0(\theta)|\Psi_0\rangle + q_1(\theta)|\Psi_1\rangle + q_2(\theta)|\Psi_2\rangle, \quad (\text{B7})$$

where the new coefficients are given as

$$\begin{aligned} q_0(\theta) &= p_0 \cos^2(\theta) + \sqrt{2} p_1 \cos(\theta) \sin(\theta) + p_2 \sin^2(\theta), \\ q_1(\theta) &= \frac{1}{\sqrt{2}} \sin(2\theta)(p_2 - p_0) + \frac{1}{\sqrt{2}} \cos(2\theta) p_1, \\ q_2(\theta) &= p_0 \sin^2(\theta) - \sqrt{2} p_1 \cos(\theta) \sin(\theta) + p_2 \cos^2(\theta). \end{aligned} \quad (\text{B8})$$

First of all, we notice that $q_1(\theta)$ can always be set to 0 for some choice of θ . Therefore we can without loss of generality always assume that there is a basis such that the amplitude of $|\Psi_1\rangle$ is 0 and $p_0, p_2 > 0$. That is, a general singlet state becomes

$$|\Psi(\mathbf{p})\rangle = p_0|\Psi_0\rangle + p_2|\Psi_2\rangle. \quad (\text{B9})$$

We will use this orbital basis as the reference basis, and the transformed amplitudes simplify to

$$\begin{aligned} q_0(\theta) &= p_0 \cos^2(\theta) + p_2 \sin^2(\theta), \\ q_1(\theta) &= \sqrt{2} \cos(\theta) \sin(\theta)(p_2 - p_0), \\ q_2(\theta) &= p_0 \sin^2(\theta) + p_2 \cos^2(\theta). \end{aligned} \quad (\text{B10})$$

Specially, $p_0 = p_2 = 1/\sqrt{2}$ is a stationary point.

Second, the orbital entropy is minimal in the reference orbital basis, where the eigenvalues of the orbital RDMS are simply $\{p_0^2, p_2^2, 0, 0\}$, and the minimal entropy is given by

$$S(\rho_{1/2}(\mathbf{p})) = -p_0^2 \log(p_0^2) - p_2^2 \log(p_2^2). \quad (\text{B11})$$

In a transformed orbital basis, the spectrum of the orbital RDMS is

$$\text{Spec}(\rho_{1/2}(\mathbf{p}, \theta)) = \left\{ q_0(\theta)^2, \frac{q_1(\theta)^2}{2}, \frac{q_1(\theta)^2}{2}, q_2(\theta)^2 \right\}. \quad (\text{B12})$$

The largest eigenvalue of the RDMS is given by $\max q_0(\theta)^2, q_2(\theta)^2$, since

$$\begin{aligned} \max\{q_0(\theta), q_2(\theta)\} &\geq \frac{q_0(\theta) + q_2(\theta)}{2} \\ &= \frac{p_0(\theta) + p_2(\theta)}{2} \\ &\geq \left| \frac{q_1(\theta)}{\sqrt{2}} \right|. \end{aligned} \quad (\text{B13})$$

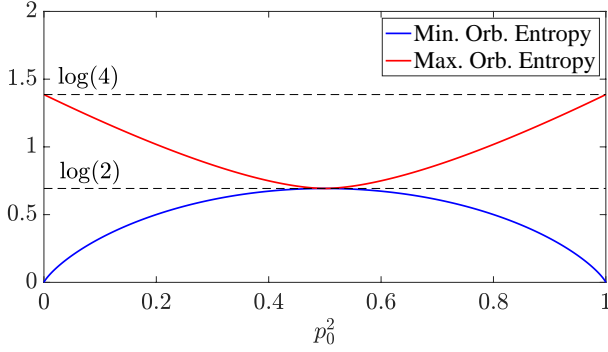


FIG. 7: Minimal/maximal orbital entropy $S(\rho_{1/2})$ over all real orbital basis, against the amplitude p_0^2 in (B9).

Additionally, it is easy to see that $p_0^2 \geq \max q_0(\theta)^2, q_2(\theta)^2$. We can therefore easily conclude that the spectrum of the RDMs at $\theta = 0$ majorizes all other possible spectra, and that when $\theta = 0$ the orbital entropy is at its lowest.

Third, maximal orbital entropy is achieved by a $\frac{\pi}{4}$ -rotation from the reference orbitals. When $\theta = \frac{\pi}{4}$, the spectrum of the RDMs is given by

$$\text{Spec}\left(\rho_{1/2}\left(\mathbf{p}, \frac{\pi}{4}\right)\right) = \left\{ \left(\frac{p_0 + p_2}{2}\right)^2, \left(\frac{p_0 - p_2}{2}\right)^2, \left(\frac{p_0 - p_2}{2}\right)^2, \left(\frac{p_0 + p_2}{2}\right)^2 \right\}. \quad (\text{B14})$$

Notice that

$$\begin{aligned} \text{Spec}(\rho_{1/2}(\mathbf{p}, \theta)) &\succ \left\{ \frac{q_0(\theta)^2 + q_2(\theta)^2}{2}, \frac{q_1(\theta)^2}{2}, \frac{q_1(\theta)^2}{2}, \frac{q_0(\theta)^2 + q_2(\theta)^2}{2} \right\} \\ &\succ \text{Spec}\left(\rho_{1/2}\left(\mathbf{p}, \frac{\pi}{4}\right)\right). \end{aligned} \quad (\text{B15})$$

Therefore the orbital entropy is maximal when $\theta = \frac{\pi}{4}$, which equals to

$$\begin{aligned} S\left(\rho_{1/2}\left(\mathbf{p}, \frac{\pi}{4}\right)\right) &= -2 \left(\frac{p_0 + p_2}{2}\right)^2 \log \left[\left(\frac{p_0 + p_2}{2}\right)^2 \right] \\ &\quad - 2 \left(\frac{p_0 - p_2}{2}\right)^2 \log \left[\left(\frac{p_0 - p_2}{2}\right)^2 \right]. \end{aligned} \quad (\text{B16})$$

To summarize, through orbital rotation, one can minimize/maximize the orbital entropy of the two-electron state, which in this case coincide with a measure of multireference character, namely the CI entropy. The orbital entropy is minimized when $|\Psi\rangle$ is expressed in a zero seniority form, and is maximized when a $\frac{\pi}{4}$ -rotation

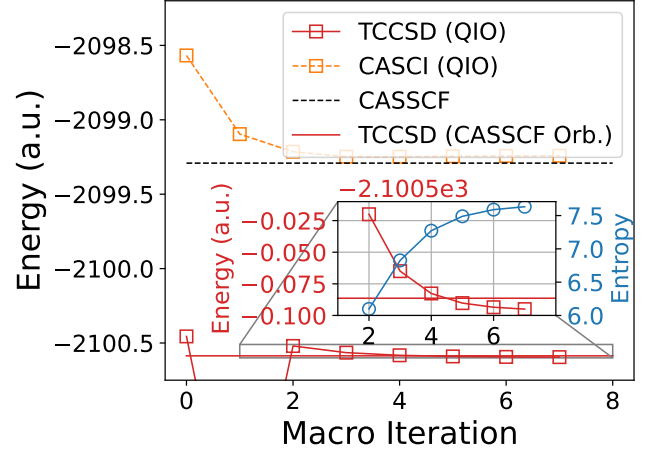


FIG. 8: TCCSD-QIO optimization of the Cr_2 molecule at the bond length of 1.679 Å in the cc-pV5Z-DK basis set, consisting of 306 orbitals. A minimal active space of (12,12) is used. The inset shows the details of the TCCSD energies and the total orbital correlation as the orbitals are optimized.

is applied to the minimizing orbital basis. These findings are encapsulated in Figure 7, where we presented the minimal/maximal single orbital entropy $S(\rho_{1/2})$ over all real orbital basis, against the amplitude p_0^2 . When $p_0^2 = 0, 1$, the state is a single Slater determinant, and correspondingly the minimal orbital entropy vanishes. As p_0^2 approaches 1/2, $|\Psi\rangle$ becomes more multireference, and accordingly the minimal orbital entropy increases. When $p_0^2 = 1/2$, the two orbitals are equally correlated/entangled in every orbital basis. In other words, the complexity of the state cannot be transformed away by orbital rotation. In contrast, the maximal orbital entropy behaves in the opposite manner. It is maximal when $p_0^2 = 0, 1$, and minimal when $p_0^2 = 1/2$. It signals the triviality of the orbital correlation of a single reference state in a poorly chosen orbital basis.

Appendix C: TCCSD-QIO optimization of Cr_2

In the original QICAS paper [73], a truncated set of orbitals were used due to the huge computational cost of low-bond DMRG calculation. We also point out that the CASSCF algorithm in this case also gets very expensive. As the optimization proceeds, the active space CASCI energies decrease and eventually converge slightly above the CASSCF energy, while the TCCSD energies decrease below the one using CASSCF canonical orbitals. The abrupt decrease in the TCCSD energy at iteration 1 results from the orbital rotation traversing a region where the reference determinant isn't dominant, and the tailored MP2 (TMP2) ansatz is employed to navigate out of this region. Even at the equilibrium bond length, the

wavefunction exhibits a large amount of multi-reference character, as indicated by the large reduction of roughly 700 mHa in the CASCI energy in the active space alone from the initial HF orbitals to the final QIO orbitals. The

difference between the CASCI and TCCSD energies can be considered as the dynamic correlation energy, which is on the order of 1000 mHa across the optimization.

Appendix D: Original Data

See TABLE I for the original data of the C_2 molecule and TABLE II for the original data of the Cr_2 molecule presented in Figure 6 in the main text.

C-C (Bohr)	QIO	TCCSD-NO	CASSCF-NO	UCCSD-NO	HFO	F_{QIO}
1.8	-75.4537845	-75.4538515	-75.451787	-75.4505035	-75.4477625	2.775
2.0	-75.6339123	-75.6338969	-75.631530	-75.6304366	-75.6281571	2.987
2.2	-75.7105573	-75.7102883	-75.707881	-75.7067405	-75.7047199	3.190
2.4	-75.7284669	-75.7281048	-75.725810	-75.7244722	-75.7226391	3.384
2.6	-75.7151864	-75.7145051	-75.712407	-75.7108455	-75.7092274	3.575
2.8	-75.6858595	-75.6858930	-75.684042	-75.6823171	-75.6811697	3.634
3.0	-75.6522752	-75.6521957	-75.650593	-75.6487491	-75.6485821	3.725
3.2	-75.6342023	-75.6345553	-75.632930	-75.6334080	-75.6296234	2.466
3.4	-75.6143219	-75.6144370	-75.612805	-75.6131546	-75.6097061	2.607
3.6	-75.5952101	-75.5951644	-75.593422	-75.5935781	-75.5904149	2.764
3.8	-75.5779611	-75.5777775	-75.575879	-75.5757977	-75.5728311	2.937
4.0	-75.5630263	-75.5628871	-75.560785	-75.5604078	-75.5575338	3.133
4.2	-75.5508078	-75.5507175	-75.548390	-75.5477326	-75.5447838	3.361
4.4	-75.5412382	-75.5412656	-75.538661	-75.5378033	-75.5346044	3.628
4.6	-75.5340541	-75.5341825	-75.531360	-75.5304352	-75.5268035	3.922
4.8	-75.5288546	-75.5290184	-75.526062	-75.5251912	-75.5210413	4.220
5.0	-75.5250909	-75.5252870	-75.522268	-75.5215623	-75.5168579	4.496
5.2	-75.5223409	-75.5225585	-75.519520	-75.5190494	-75.5138422	4.732
5.4	-75.5202896	-75.5204730	-75.517464	-75.5172273	-75.5116615	4.925
5.6	-75.5186942	-75.5188673	-75.515894	-75.5158398	-75.5100565	5.077
5.8	-75.5174429	-75.5175640	-75.514640	-75.5147167	-75.5088626	5.196

TABLE I: TCCSD energy and total orbital correlation for C_2 presented in Fig. 5 in the main text. Energy in Hartree.

Cr-Cr (\AA)	QIO	TCCSD-NO	CASSCF-NO	UCCSD-NO	F_{QIO}
1.50	-2099.8682088	-2099.8665733	-2099.8604731	-2099.8505611	5.869
1.55	-2099.8805779	-2099.8790180	-2099.8715983	-2099.8594378	6.159
1.57	N/A	N/A	-2099.8741577	-2099.8609289	N/A
1.60	-2099.8869346	-2099.8855955	-2099.8765241	-2099.8614968	6.514
1.64	-2099.8895896	-2099.8882957	-2099.8777240	-2099.8598751	6.853
1.68	-2099.8907057	-2099.8896679	-2099.8774932	-2099.8564156	7.226
1.73	-2099.8910933	-2099.8903517	-2099.8761989	-2099.8506864	7.719
1.80	-2099.8908079	-2099.8903717	-2099.8735534	-2099.8422357	8.386
1.90	-2099.8897337	N/A	-2099.8690127	-2099.8338818	9.175
2.00	N/A	N/A	-2099.8633707	-2099.8345337	N/A

TABLE II: TCCSD energy and total orbital correlation for Cr_2 presented in Figure 6 in the main text. Energy in Hartree.

- [1] S. Sharma, K. Sivalingam, F. Neese, and G. K.-L. Chan, Low-energy spectrum of iron–sulfur clusters directly from many-particle quantum mechanics, *Nat. Chem.* **6**, 927 (2014).
- [2] Y. Kurashige, G. K.-L. Chan, and T. Yanai, Entangled quantum electronic wavefunctions of the Mn₄CaO₅ cluster in photosystem II, *Nat. Chem.* **5**, 660 (2013).
- [3] G. H. Booth, A. Grüneis, G. Kresse, and A. Alavi, Towards an exact description of electronic wavefunctions in real solids., *Nature* **493**, 365 (2013), 23254929.
- [4] N. A. Bogdanov, G. Li Manni, S. Sharma, O. Gunnarsson, and A. Alavi, Enhancement of superexchange due to synergetic breathing and hopping in corner-sharing cuprates, *Nat. Phys.* **18**, 190 (2022).
- [5] Z.-H. Cui, H. Zhai, X. Zhang, and G. K.-L. Chan, Systematic electronic structure in the cuprate parent state from quantum many-body simulations, *Science* **377**, 1192 (2022).
- [6] T. Kato, On the eigenfunctions of many-particle systems in quantum mechanics, *Commun. Pure Appl. Math.* **10**, 151 (1957).
- [7] J. J. Shepherd and A. Grüneis, Many-body quantum chemistry for the electron gas: Convergent perturbative theories, *Phys. Rev. Lett.* **110**, 10.1103/PhysRevLett.110.226401 (2013), arxiv:1310.6059.
- [8] M. Ochi, R. Arita, and S. Tsuneyuki, Correlated Band Structure of a Transition Metal Oxide ZnO Obtained from a Many-Body Wave Function Theory, *Phys. Rev. Lett.* **118**, 026402 (2017).
- [9] N. Masios, A. Irmeler, T. Schäfer, and A. Grüneis, Averting the Infrared Catastrophe in the Gold Standard of Quantum Chemistry, *Phys. Rev. Lett.* **131**, 186401 (2023).
- [10] V. A. Neufeld and T. C. Berkelbach, Highly Accurate Electronic Structure of Metallic Solids from Coupled-Cluster Theory with Nonperturbative Triple Excitations, *Phys. Rev. Lett.* **131**, 186402 (2023).
- [11] N. D. Drummond and R. J. Needs, Van der Waals Interactions between Thin Metallic Wires and Layers, *Phys. Rev. Lett.* **99**, 166401 (2007).
- [12] A. Tkatchenko, R. A. DiStasio, R. Car, and M. Scheffler, Accurate and Efficient Method for Many-Body van der Waals Interactions, *Phys. Rev. Lett.* **108**, 236402 (2012).
- [13] J. Cioslowski, C. Schilling, and R. Schilling, 1-Matrix functional for long-range interaction energy of two hydrogen atoms, *J. Chem. Phys.* **158**, 084106 (2023).
- [14] U. Schollwöck, The density-matrix renormalization group, *Rev. Mod. Phys.* **77**, 259 (2005).
- [15] G. K.-L. Chan and S. Sharma, The Density Matrix Renormalization Group in Quantum Chemistry, *Annu. Rev. Phys. Chem.* **62**, 465 (2011).
- [16] A. Baiardi and M. Reiher, The density matrix renormalization group in chemistry and molecular physics: Recent developments and new challenges, *J. Chem. Phys.* **152**, 040903 (2020).
- [17] G. H. Booth, A. J. Thom, and A. Alavi, Fermion monte carlo without fixed nodes: A game of life, death, and annihilation in Slater determinant space, *J. Chem. Phys.* **131**, 054106 (2009).
- [18] D. Cleland, G. H. Booth, and A. Alavi, Communications: Survival of the fittest: Accelerating convergence in full configuration-interaction quantum Monte Carlo, *J. Chem. Phys.* **132**, 10.1063/1.3302277 (2010).
- [19] G. Li Manni, S. D. Smart, and A. Alavi, Combining the Complete Active Space Self-Consistent Field Method and the Full Configuration Interaction Quantum Monte Carlo within a Super-CI Framework, with Application to Challenging Metal-Porphyrins, *J. Chem. Theory Comput.* **12**, 1245 (2016).
- [20] H. Shi and S. Zhang, Some recent developments in auxiliary-field quantum Monte Carlo for real materials, *J. Chem. Phys.* **154**, 024107 (2021).
- [21] J. Lee, H. Q. Pham, and D. R. Reichman, Twenty Years of Auxiliary-Field Quantum Monte Carlo in Quantum Chemistry: An Overview and Assessment on Main Group Chemistry and Bond-Breaking, *J. Chem. Theory Comput.* **18**, 7024 (2022).
- [22] K. Andersson, P.-Å. Malmqvist, and B. O. Roos, Second-order perturbation theory with a complete active space self-consistent field reference function, *J. Chem. Phys.* **96**, 1218 (1992).
- [23] C. Angeli, R. Cimraglia, S. Evangelisti, T. Leininger, and J.-P. Malrieu, Introduction of n -electron valence states for multireference perturbation theory, *J. Chem. Phys.* **114**, 10252 (2001).
- [24] G. Li Manni, R. K. Carlson, S. Luo, D. Ma, J. Olsen, D. G. Truhlar, and L. Gagliardi, Multiconfiguration Pair-Density Functional Theory, *J. Chem. Theory Comput.* **10**, 3669 (2014).
- [25] L. Gagliardi, D. G. Truhlar, G. Li Manni, R. K. Carlson, C. E. Hoyer, and J. L. Bao, Multiconfiguration Pair-Density Functional Theory: A New Way To Treat Strongly Correlated Systems, *Acc. Chem. Res.* **50**, 66 (2017).
- [26] R. Bartlett and M. Musiał, Coupled-cluster theory in quantum chemistry, *Rev. Mod. Phys.* **79**, 291 (2007).
- [27] D. Kats and F. R. Manby, Communication: The distinguishable cluster approximation, *J. Chem. Phys.* **139**, 021102 (2013).
- [28] D. Kats, Communication: The distinguishable cluster approximation. II. The role of orbital relaxation, *J. Chem. Phys.* **141**, 061101 (2014).
- [29] T. Gruber, K. Liao, T. Tsatsoulis, F. Hummel, and A. Grüneis, Applying the Coupled-Cluster Ansatz to Solids and Surfaces in the Thermodynamic Limit, *Phys. Rev. X*, **8**, 21043 (2018).
- [30] D. Kats and A. Köhn, On the distinguishable cluster approximation for triple excitations, *J. Chem. Phys.* **150** (2019).
- [31] W. Yang, Y. Zhang, and P. W. Ayers, Degenerate Ground States and a Fractional Number of Electrons in Density and Reduced Density Matrix Functional Theory, *Phys. Rev. Lett.* **84**, 5172 (2000).
- [32] D. A. Mazziotti, Anti-Hermitian Contracted Schrödinger Equation: Direct Determination of the Two-Electron Reduced Density Matrices of Many-Electron Molecules, *Phys. Rev. Lett.* **97**, 143002 (2006).
- [33] D. A. Mazziotti, Parametrization of the Two-Electron Reduced Density Matrix for its Direct Calculation without the Many-Electron Wave Function, *Phys. Rev. Lett.* **101**, 253002 (2008).

- [34] C. Schilling and S. Pittalis, Ensemble Reduced Density Matrix Functional Theory for Excited States and Hierarchical Generalization of Pauli’s Exclusion Principle, *Phys. Rev. Lett.* **127**, 023001 (2021).
- [35] E. Neuscamman, T. Yanai, and G. K.-L. Chan, A review of canonical transformation theory, *Int. Rev. Phys. Chem.* **29**, 231 (2010).
- [36] H. Luo and A. Alavi, Combining the Transcorrelated Method with Full Configuration Interaction Quantum Monte Carlo: Application to the Homogeneous Electron Gas, *J. Chem. Theory Comput.* **14**, 1403 (2018).
- [37] E. Vitale, A. Alavi, and D. Kats, FCIQMC-Tailored Distinguishable Cluster Approach, *J. Chem. Theory Comput.* **16**, 5621 (2020).
- [38] K. Liao, T. Schraivogel, H. Luo, D. Kats, and A. Alavi, Towards efficient and accurate ab initio solutions to periodic systems via transcorrelation and coupled cluster theory, *Phys. Rev. Res.* **3**, 033072 (2021).
- [39] T. Schraivogel, A. J. Cohen, A. Alavi, and D. Kats, Transcorrelated coupled cluster methods, *J. Chem. Phys.* **155**, 191101 (2021).
- [40] A. Baiardi, M. Lesiuk, and M. Reiher, Explicitly Correlated Electronic Structure Calculations with Transcorrelated Matrix Product Operators, *J. Chem. Theory Comput.* **18**, 4203 (2022).
- [41] K. Liao, H. Zhai, E. M. Christmaier, T. Schraivogel, P. L. Ríos, D. Kats, and A. Alavi, Density Matrix Renormalization Group for Transcorrelated Hamiltonians: Ground and Excited States in Molecules, *J. Chem. Theory Comput.* **19**, 1734 (2023).
- [42] P.-O. Löwdin, Quantum Theory of Many-Particle Systems. I. Physical Interpretations by Means of Density Matrices, Natural Spin-Orbitals, and Convergence Problems in the Method of Configurational Interaction, *Phys. Rev.* **97**, 1474 (1955).
- [43] A. G. Taube and R. J. Bartlett, Frozen Natural Orbitals: Systematic Basis Set Truncation for Coupled-Cluster Theory, *Collect. Czech. Chem. Commun.* **70**, 837 (2005).
- [44] A. G. Taube and R. J. Bartlett, Frozen natural orbital coupled-cluster theory: Forces and application to decomposition of nitroethane, *J. Chem. Phys.* **128**, 164101 (2008).
- [45] A. Grüneis, G. H. Booth, M. Marsman, J. Spencer, A. Alavi, and G. Kresse, Natural orbitals for wave function based correlated calculations using a plane wave basis set, *J. Chem. Theory Comput.* **7**, 2780 (2011).
- [46] K. Liao, X.-Z. Li, A. Alavi, and A. Grüneis, A comparative study using state-of-the-art electronic structure theories on solid hydrogen phases under high pressures, *npj Comput. Mater.* **5**, 1 (2019).
- [47] L. Kong, F. A. Bischoff, and E. F. Valeev, Explicitly Correlated R12/F12 Methods for Electronic Structure, *Chem. Rev.* **112**, 75 (2012).
- [48] Q. Ma, M. Schwilk, C. Köppl, and H.-J. Werner, Scalable Electron Correlation Methods. 4. Parallel Explicitly Correlated Local Coupled Cluster with Pair Natural Orbitals (PNO-LCCSD-F12), *J. Chem. Theory Comput.* **13**, 4871 (2017).
- [49] F. Pavošević, C. Peng, P. Pinski, C. Riplinger, F. Neese, and E. F. Valeev, SparseMaps—A systematic infrastructure for reduced scaling electronic structure methods. V. Linear scaling explicitly correlated coupled-cluster method with pair natural orbitals, *J. Chem. Phys.* **146**, 174108 (2017).
- [50] M. Kállay, R. A. Horváth, L. Gyevi-Nagy, and P. R. Nagy, Basis Set Limit CCSD(T) Energies for Extended Molecules via a Reduced-Cost Explicitly Correlated Approach, *J. Chem. Theory Comput.* **19**, 174 (2023).
- [51] W. Dobrautz, I. O. Sokolov, K. Liao, P. L. Ríos, M. Rahm, A. Alavi, and I. Tavernelli, Ab Initio Transcorrelated Method enabling accurate Quantum Chemistry on near-term Quantum Hardware (2023), arxiv:2303.02007 [cond-mat, physics:physics, physics:quant-ph].
- [52] W. Li, P. Piecuch, J. R. Gour, and S. Li, Local correlation calculations using standard and renormalized coupled-cluster approaches, *J. Chem. Phys.* **131**, 114109 (2009).
- [53] Z. Rolik, L. Szegedy, I. Ladjánszki, B. Ladóczki, and M. Kállay, An efficient linear-scaling CCSD(T) method based on local natural orbitals, *J. Chem. Phys.* **139**, 094105 (2013).
- [54] M. Srednicki, Entropy and area, *Phys. Rev. Lett.* **71**, 666 (1993).
- [55] M. B. Hastings, Entropy and entanglement in quantum ground states, *Phys. Rev. B* **76**, 035114 (2007).
- [56] J. Eisert, M. Cramer, and M. B. Plenio, Colloquium: Area laws for the entanglement entropy, *Rev. Mod. Phys.* **82**, 277 (2010).
- [57] C. Krumnow, L. Veis, Ö. Legeza, and J. Eisert, Fermionic orbital optimisation in tensor network states, *Phys. Rev. Lett.* **117**, 210402 (2016), arxiv:1504.00042 [cond-mat, physics:physics, physics:quant-ph].
- [58] G. Li Manni, W. Dobrautz, and A. Alavi, Compression of Spin-Adapted Multiconfigurational Wave Functions in Exchange-Coupled Polynuclear Spin Systems, *J. Chem. Theory Comput.* **16**, 2202 (2020).
- [59] B. O. Roos, The complete active space SCF method in a fock-matrix-based super-CI formulation, *Int. J. Quantum Chem.* **18**, 175 (1980).
- [60] P. E. M. Siegbahn, J. Almlöf, A. Heiberg, and B. O. Roos, The complete active space SCF (CASSCF) method in a Newton–Raphson formulation with application to the HNO molecule, *J. Chem. Phys.* **74**, 2384 (1981).
- [61] H. R. Larsson, H. Zhai, C. J. Umrigar, and G. K.-L. Chan, The Chromium Dimer: Closing a Chapter of Quantum Chemistry, *J. Am. Chem. Soc.* **144**, 15932 (2022).
- [62] Z. Tóth and P. Pulay, Comparison of Methods for Active Orbital Selection in Multiconfigurational Calculations, *J. Chem. Theory Comput.* **16**, 7328 (2020).
- [63] The selection of the active space in general is a very challenging task on its own, here we focus on the optimization of the orbitals within a given active space size.
- [64] J. Lee and M. Head-Gordon, Regularized Orbital-Optimized Second-Order Møller–Plesset Perturbation Theory: A Reliable Fifth-Order-Scaling Electron Correlation Model with Orbital Energy Dependent Regularizers, *J. Chem. Theory Comput.* **14**, 5203 (2018).
- [65] K. Boguslawski, P. Tecmer, Ö. Legeza, and M. Reiher, Entanglement Measures for Single- and Multireference Correlation Effects, *J. Phys. Chem. Lett.* **3**, 3129 (2012).
- [66] K. Boguslawski and P. Tecmer, Orbital entanglement in quantum chemistry, *Int. J. Quantum Chem.* **115**, 1289 (2015).
- [67] C. J. Stein and M. Reiher, Automated Selection of Active Orbital Spaces, *J. Chem. Theory Comput.* **12**, 1760

- (2016).
- [68] C. J. Stein and M. Reiher, Measuring multi-configurational character by orbital entanglement, *Mol. Phys.* **115**, 2110 (2017).
- [69] L. Ding and C. Schilling, Correlation Paradox of the Dissociation Limit: A Quantum Information Perspective, *J. Chem. Theory Comput.* **16**, 4159 (2020).
- [70] L. Ding, S. Mardazad, S. Das, S. Szalay, U. Schollwöck, Z. Zimborás, and C. Schilling, Concept of Orbital Entanglement and Correlation in Quantum Chemistry, *J. Chem. Theory Comput.* **17**, 79 (2021).
- [71] L. Henderson and V. Vedral, Classical, quantum and total correlations, *J. Phys. A: Math. Gen.* **34**, 6899 (2001).
- [72] B. Groisman, S. Popescu, and A. Winter, Quantum, classical, and total amount of correlations in a quantum state, *Phys. Rev. A* **72**, 032317 (2005).
- [73] L. Ding, S. Knecht, and C. Schilling, Quantum Information-Assisted Complete Active Space Optimization (QICAS), *J. Phys. Chem. Lett.* **14**, 11022 (2023).
- [74] K. Modi, T. Paterek, W. Son, V. Vedral, and M. Williamson, Unified View of Quantum and Classical Correlations, *Phys. Rev. Lett.* **104**, 080501 (2010).
- [75] N. Gigena and R. Rossignoli, Entanglement in fermion systems, *Phys. Rev. A* **92**, 042326 (2015).
- [76] T. Kinoshita, O. Hino, and R. J. Bartlett, Coupled-cluster method tailored by configuration interaction, *J. Chem. Phys.* **123**, 074106 (2005).
- [77] H. Zhai, H. R. Larsson, S. Lee, Z.-H. Cui, T. Zhu, C. Sun, L. Peng, R. Peng, K. Liao, J. Tölle, J. Yang, S. Li, and G. K.-L. Chan, BLOCK2 : A comprehensive open source framework to develop and apply state-of-the-art DMRG algorithms in electronic structure and beyond, *J. Chem. Phys.* **159**, 234801 (2023).
- [78] QIO: Quantum information-assisted orbital optimization package. Accessed on March 21st, 2024., Christian Schilling Group (2024).
- [79] Q. Sun, X. Zhang, S. Banerjee, P. Bao, M. Barbry, N. S. Blunt, N. A. Bogdanov, G. H. Booth, J. Chen, Z.-H. Cui, J. J. Eriksen, Y. Gao, S. Guo, J. Hermann, M. R. Hermes, K. Koh, P. Koval, S. Lehtola, Z. Li, J. Liu, N. Mardirossian, J. D. McClain, M. Motta, B. Mussard, H. Q. Pham, A. Pulkin, W. Purwanto, P. J. Robinson, E. Ronca, E. R. Sayfutyarova, M. Scheurer, H. F. Schurkus, J. E. T. Smith, C. Sun, S.-N. Sun, S. Upadhyay, L. K. Wagner, X. Wang, A. White, J. D. Whitfield, M. J. Williamson, S. Wouters, J. Yang, J. M. Yu, T. Zhu, T. C. Berkelbach, S. Sharma, A. Y. Sokolov, and G. K.-L. Chan, Recent developments in the PySCF program package, *J. Chem. Phys.* **153**, 024109 (2020).
- [80] S. Wouters, W. Poelmans, P. W. Ayers, and D. Van Neck, CheMPS2: A free open-source spin-adapted implementation of the density matrix renormalization group for ab initio quantum chemistry, *Comput. Phys. Commun.* **185**, 1501 (2014).
- [81] W. Kutzelnigg and W. Liu, Quasirelativistic theory equivalent to fully relativistic theory, *J. Chem. Phys.* **123**, 241102 (2005).
- [82] D. Peng and M. Reiher, Exact decoupling of the relativistic Fock operator, *Theor. Chem. Acc.* **131**, 1081 (2012).
- [83] B. O. Roos, The Ground State Potential for the Chromium Dimer Revisited, *Collect. Czech. Chem. Commun.* **68**, 265 (2003).
- [84] Y. Kurashige and T. Yanai, Second-order perturbation theory with a density matrix renormalization group self-consistent field reference function: Theory and application to the study of chromium dimer, *J. Chem. Phys.* **135**, 094104 (2011).
- [85] K. Hongo and R. Maezono, A benchmark quantum Monte Carlo study of the ground state chromium dimer, *Int. J. Quantum Chem.* **112**, 1243 (2012).
- [86] G. Li Manni, D. Ma, F. Aquilante, J. Olsen, and L. Gagliardi, SplitGAS Method for Strong Correlation and the Challenging Case of Cr₂, *J. Chem. Theory Comput.* **9**, 3375 (2013).
- [87] Y. Yamada, K. Hongo, K. Egashira, Y. Kita, U. Nagashima, and M. Tachikawa, Gold-standard coupled-cluster study of the ground-state chromium dimer cation, *Chem. Phys. Lett.* **555**, 84 (2013).
- [88] W. Purwanto, S. Zhang, and H. Krakauer, An auxiliary-field quantum Monte Carlo study of the chromium dimer, *J. Chem. Phys.* **142**, 064302 (2015).
- [89] S. Vancoillie, P. Á. Malmqvist, and V. Veryazov, Potential Energy Surface of the Chromium Dimer Re-revisited with Multiconfigurational Perturbation Theory, *J. Chem. Theory Comput.* **12**, 1647 (2016).
- [90] A. Leszczyk, M. Máté, Ö. Legeza, and K. Boguslawski, Assessing the Accuracy of Tailored Coupled Cluster Methods Corrected by Electronic Wave Functions of Polynomial Cost, *J. Chem. Theory Comput.* **18**, 96 (2022).
- [91] W. Kutzelnigg and D. Mukherjee, Cumulant expansion of the reduced density matrices, *J. Chem. Phys.* **110**, 2800 (1999).
- [92] D. A. Mazziotti, Approximate solution for electron correlation through the use of Schwinger probes, *Chemical Physics Letters* **289**, 419 (1998).
- [93] L. Veis, A. Antalík, J. Brabec, F. Neese, Ö. Legeza, and J. Pittner, Coupled Cluster Method with Single and Double Excitations Tailored by Matrix Product State Wave Functions, *J. Phys. Chem. Lett.* **7**, 4072 (2016).